Dopant Segregation in Single-Crystal Optical Fiber Grown via the Laser-Heated Pedestal Growth Technique

Gary Lander[1,2]*; Jeffrey Wuenschell[3,4]; Geunsik Lim[1,2]; Dolendra Karki[5]; Jun Young Hong[5]; Paul Ohodnicki, Jr.[5]; Michael Buric[1]

[1]National Energy Technology Laboratory, 3610 Collins Ferry Road, Morgantown, WV 26505, USA
[2]NETL Support Contractor, 3610 Collins Ferry Road, Morgantown, WV 26505, USA
[3]National Energy Technology Laboratory, 626 Cochran Mill Road, Pittsburgh, PA 15236, USA
[4]NETL Support Contractor, 626 Cochran Mill Road, Pittsburgh, PA 15236, USA
[5]University of Pittsburgh, 4200 Fifth Avenue, Pittsburgh, PA 15260, USA

ABSTRACT

Single crystal (SC) optical fiber has promising potential to be used for optical fiber sensing applications in harsh conditions due to its robustness to high temperature, high radioactivity, and resistance to chemical corrosion as compared to optical sensors using silica fiber. However, SC fiber grown via the laser-heated pedestal growth (LHPG) technique innately does not have a core-cladding structure found in standard optical fiber, resulting in optical losses. In this work we investigate optimization of the growth parameters of a two LHPG process used to grow SC fiber with a graded index via introduction of dopants to the feedstock material. Feedstock material is fabricated with the first LHPG device, then sol-gel dip-coated to create outer films of dopant material. The dip-coated feedstock is used to grow SC fiber in which segregation of the dopant constituents occurs, resulting in a graded index of refraction across the fiber, and an effective core-cladding structure. Hardware and software improvements to both LHPG systems are presented and the growth parameters for short pieces of ~320-330 μm diameter YAG fiber has been established. Characterization techniques/procedures have also been established for future grown SC fiber. These improvements and preparations are anticipated to result in a significant increase in grown fiber quality with a similar growth rate to that previously established.

Keywords: laser-heated pedestal growth, optical fiber, single-crystal, dopant segregation, growth from melt, rare-earth doped materials, Raman

*gary.lander@netl.doe.gov

1. INTRODUCTION

Optical fibers are extensively used for a multitude of different sensing applications. One advantage to many electronic sensors is their capability to be used with pulsed lasers to construct distributed sensors, as opposed to arrays of point-based sensors, allowing for improved resolution. Regarding sensing in harsh environments, optical fiber sensors provide the advantage of robustness due to the resiliency of glass and ceramics to chemically damaging conditions and/or high temperatures, as opposed to electronic sensors which require metallic interconnects and leads. The most common material used in optical fibers is silica and/or doped silica. Silica optical fibers exhibit great transmittivity in the visible and telecom wavelength ranges and are deployable in a wide range of applications. However, they are susceptible to damage and critical failure in very harsh conditions. For example, off-the-shelf silica glass fiber is typically limited to operation under 500-900 °C, due to embrittlement and material degradation pathways, such as crystallization and dopant diffusion that occur at high temperatures.

However, optical fibers composed of single-crystal (SC) material can maintain functionality under chemically-corrosive, high-radioactivity, and high-temperature environments that silica fiber cannot. In regard to temperature, single-crystal fibers can be used to make sensors that are operational well above 1000 °C [1, 2]. Indeed, SC material can be used in a functional optical sensor up to the material's melting point, which is roughly 2000 °C for commonly

grown sapphire (α-Al_2O_3) and yttrium aluminum garnet (YAG) fibers. This makes sapphire and YAG optical fibers ideal for sensing in harsh environments such as in jet engines, boilers, and nuclear reactors [3].

A standard optical fiber is composed of a core and surrounding cladding layer made of two different optical media. The core material has a higher index of refraction than the surrounding cladding layer, inducing total internal reflection and waveguiding for an optical mode inside the core. In this work, we grow SC optical fiber to be used as optical sensors in harsh environments via the laser-heated pedestal growth (LHPG) technique. When the host material used for LHPG is a pure-crystalline material, the resulting fiber lacks a standard core-cladding structure. Thus, although SC optical fiber is much more robust to harsh conditions than silica fiber, its transmittivity is lower due to the poor waveguiding capabilities as compared to optical fiber with a core-cladding structure. Research is ongoing to improve the scalability of SC fiber fabrication as well as implementation of an effective core-cladding structure [4,5].

The core-cladding structure is not only essential for good waveguiding properties, but it also reduces the modal volume necessary for distributed sensing applications [6], and cladding pumping scenarios in high-power laser applications [7]. Investigations have been conducted regarding implementation of glass cladding layers on SC fiber [8,9]. However, significant losses and ultimate long-term degradation is likely due to differences in the mechanical and thermal properties of SC material vs. glass. Thus, it is imperative to develop SC cladding layers to maintain a crystalline structure across the fiber.

Two-step processes have been proposed to grow SC cladding layers on already existing SC fiber [1], but such a fabrication technique results in significant losses at the core-cladding interface as well as increases the time and cost of fabrication. Additionally, recent research has shown that the length of the grown fiber, the cladding thickness, temperature stability, and ultimately the fiber quality is significantly limited using the two-step process [1, 7, 10-12]. Thus, a single step process is more desirable. In this work, we implement in-situ fabrication of a graded refractive index fiber by leveraging crystal growth melt dynamics.

Investigations have shown that certain LHPG-grown crystal fibers exhibit a non-uniform radial distribution of dopant species [13]. The dopant constituents can migrate and segregate either toward the middle of the grown fiber or toward the outside, depending on the specific specimens involved. For example, for magnesium doped sapphire, Mg^{2+} tends to segregate toward the center during LHPG [13]. Similar effects have been noted for LHPG using YAG as the host crystal. For neodymium doped YAG, Nd^{3+} ions were observed to segregate toward the center [14,15], while for chromium doped YAG the Cr^{4+} ions were observed to segregate toward the periphery [16].

The degree of segregation and whether the dopant constituents segregate toward the center or toward the outside of the grown fiber during LHPG depends on two factors [17]. The degree of segregation is quantified as the segregation coefficient, k. The segregation coefficient is dependent on the ratio of the solubility of the dopant species in the solid phase to its solubility in the liquid phase, as well as the relative ionic size of the dopant species with respect to the ionic size of the specimen it substitutionally replaces in the host crystal. When $k = 1$ no segregation occurs and a homogeneous mix of the dopant throughout the melt occurs. When $k < 1$, dopant constituents tend to migrate toward the center, whereas toward the periphery for $k > 1$. The ratio of the ionic size of the dopant with that of the specimen it replaces is inversely related to k. That is, dopants with ionic radii greater than that which it replaces tend to migrate toward the center, and vice versa for dopants with small ionic radii. Expansion on the dynamics inside the melt was presented in previous work [18].

The closer k is to unity the smaller the degree of segregation. To fabricate fibers with good optical properties one can explore either dopants that increase the index of refraction relative to the host crystal and migrate toward the center, or those that decrease the index of refraction and migrate toward the periphery. In this work, we investigate two different dopants that we expect to migrate toward the center, creating an effective higher-index core, in both sapphire and YAG.

2. EXPERIMENTAL TECHNIQUE

Laser-Heated Pedestal Growth (LHPG)

In this work, we investigate fabrication of SC optical fiber with a core-cladding structure using two custom-built LHPG apparatuses. Details of either apparatus are presented in a previous publication [19]. A schematic of a LHPG apparatus is depicted in Figure 1.

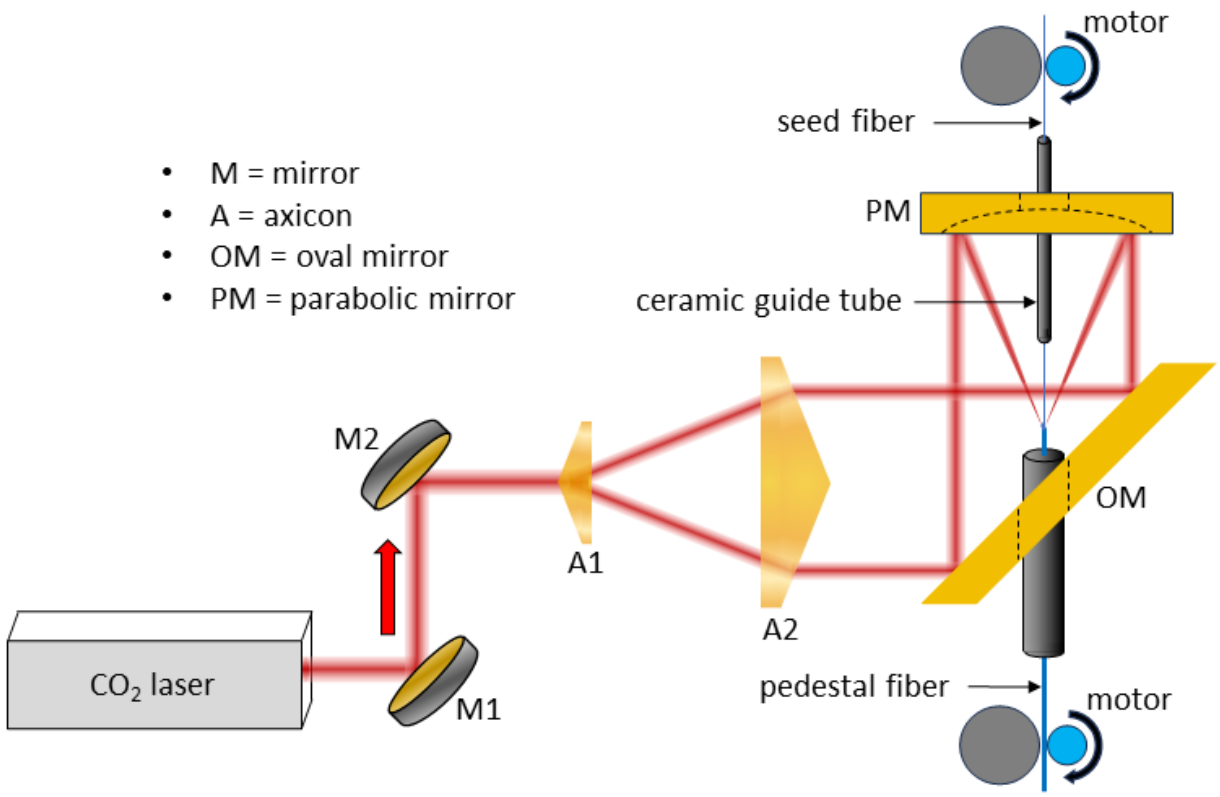

Figure 1: Schematic of either of the custom-built LHPG devices. A CO_2 laser is used as a heat source to melt SC material from which SC fiber is grown. The laser is focused onto the top of a pedestal fiber, creating a small melt, or molten zone. A seed fiber is dipped into the molten zone and as it is pulled upwards material from the molten zone solidifies, forming fiber composed of a single crystal.

For both LHPG devices a stabilized CO_2 laser is used as a heat source to melt SC material from which SC fiber is grown. The laser beam is first sent through a periscope to elevate the optical axis to make room to ultimately feed the pedestal fiber. After propagation through the periscope, the beam is sent through a ZnSe axicon telescope, which turns the Gaussian beam into a collimated "donut" shape as well as expands the beam. The beam is then reflected off an oval mirror angled 45 degrees with respect to the optical axis of the axicon telescope and is reflected upwards toward an elliptical mirror which focuses the beam onto the top of the pedestal fiber, creating a small volume of molten material (melt or molten zone). The pedestal fiber is fed up through a hole in the oval mirror and held vertical via installation inside a metallic guide tube that is fastened inside of a lens tube. A seed fiber is dropped through a hole in the parabolic mirror and dipped into the molten zone and is fastened in a ceramic guide tube to also keep the fiber vertical. As the seed fiber is pulled upward, material is pulled from the molten zone and crystallizes as it cools, forming optical fiber composed of SC material.

As the seed fiber is pulled upward and material is pulled from the molten zone, the pedestal fiber is also fed upwards to maintain a constant volume of molten material. Both the pedestal and seed fiber's velocities are controlled by mounting the fibers between a notched metallic wheel and a rubber wheel and controlling the angular velocity of the rubber wheel via motors. Not depicted in Figure 1, the diameter of the grown fiber directly above the molten zone is measured via two cameras mounted roughly 45 degrees with respect to the optical axis of the axicon telescope, and roughly 90 degrees from each other. A LabVIEW program with an active PID feedback loop can control the angular velocities of the two motors in real time to maintain a constant diameter of the grown fiber. In practice, the best results were obtained by keeping the seed fiber's velocity constant and varying the pedestal's velocity using the PID feedback loop. The ceramic guide tube holding the seed fiber is also rigidly attached to two piezoelectric This allows for precise translational alignment of the seed and pedestal fibers. An auto-alignment procedure has also been written into the LabVIEW software to maintain alignment of the seed fiber and the pedestal fiber based off of the camera images.

Two separate LHPG systems are used for two reasons. The ultimate desired diameter is on the order of 125 μm, which is a very common size for both sensing and telecommunication applications. However, the initial starting material are roughly 1 mm diameter commercially available crystalline rods. The first LHPG system grows roughly 300-350 μm fiber from the 1 mm rods. The second LHPG system uses the fiber grown from the first system as the pedestal fiber to ultimately grow 125 μm fiber. Using two LHPG systems not only allows for more precise control of the grown fiber's diameter and ultimately improves fiber quality, but it also allows for introduction of dopant crystalline materials.

Introduction of Dopants

Dopant materials are introduced by coating the 300-350 μm grown fiber with a sol-gel before installation into the second system as pedestal fiber. The sol-gel process is explained in detail in a previous work [20]. A diagram illustrating the full two LHPG process is depicted in Figure 2.

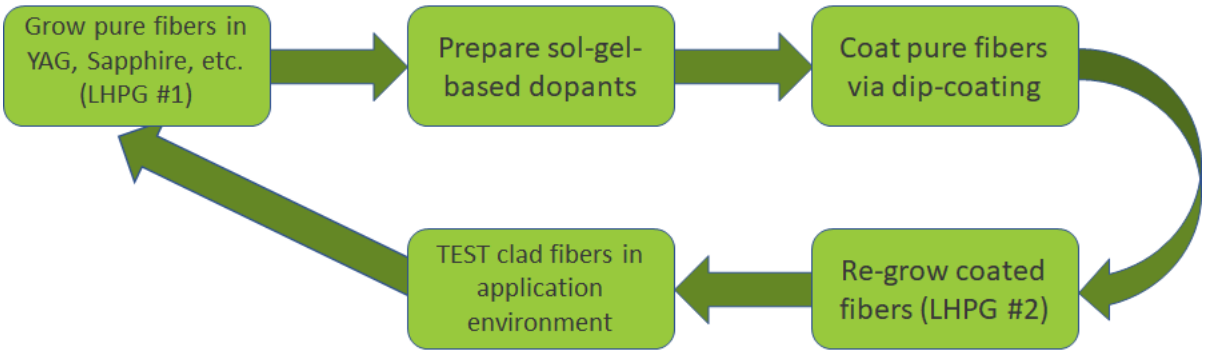

Figure 2: Diagram of the full two LHPG process used to produce doped SC optical fibers.

To coat the 300-350 μm fibers with a sufficient amount of sol-gel to introduce proper levels of dopants, a dip-coating process is repeated multiple times until of film thickness on the order of 1 μm is deposited on the outside of the fiber.

Fiber Characterization

The fibers are characterized via three different methods. Electron probe microanalysis (EPMA) is conducted on cross-sections of the grown fiber to quantify the concentrations of element constituents across the sample. EPMA is the primary method used to quantify the degree of segregation of the dopant species. The fibers' waveguiding and temperature sensing properties are characterized via measuring transmissivity and amplitudes of generated Raman signals with a custom-built Raman distributed temperature sensing (Raman-DTS) system. Lastly, the grown fibers' numerical aperture is measured with a custom-built numerical aperture (NA) measurement system.

Electron Probe Microanalysis (EPMA)

To prepare for EPMA measurements cross-sectional pieces of grown SC fiber were embedded inside fiber ferrules using UV-glue. The ferrules contained six single-crystal fibers embedded inside a 1" epoxy mount to fit into the EPMA sample holder. The sample surface was polished using an Allied Multi-prep polishing system.

Multiple images were used during the EPMA. Three different electron probe microscopy images were collected: SE, BSE, and TOPO. Some specimen concentrations were quantified via wavelength-dispersive X-ray spectroscopy (WDS), while others were quantified via energy-dispersive X-ray spectroscopy (EDS). The spectral peaks of individual specimen were cross-verified with monazite and xenotime standards.

Raman Distributed Temperature Sensing (DTS) System

A schematic of the Raman-DTS system used to measure grown SC fibers' transmittivity and ultimate efficiency as a temperature sensor is depicted in Figure 3.

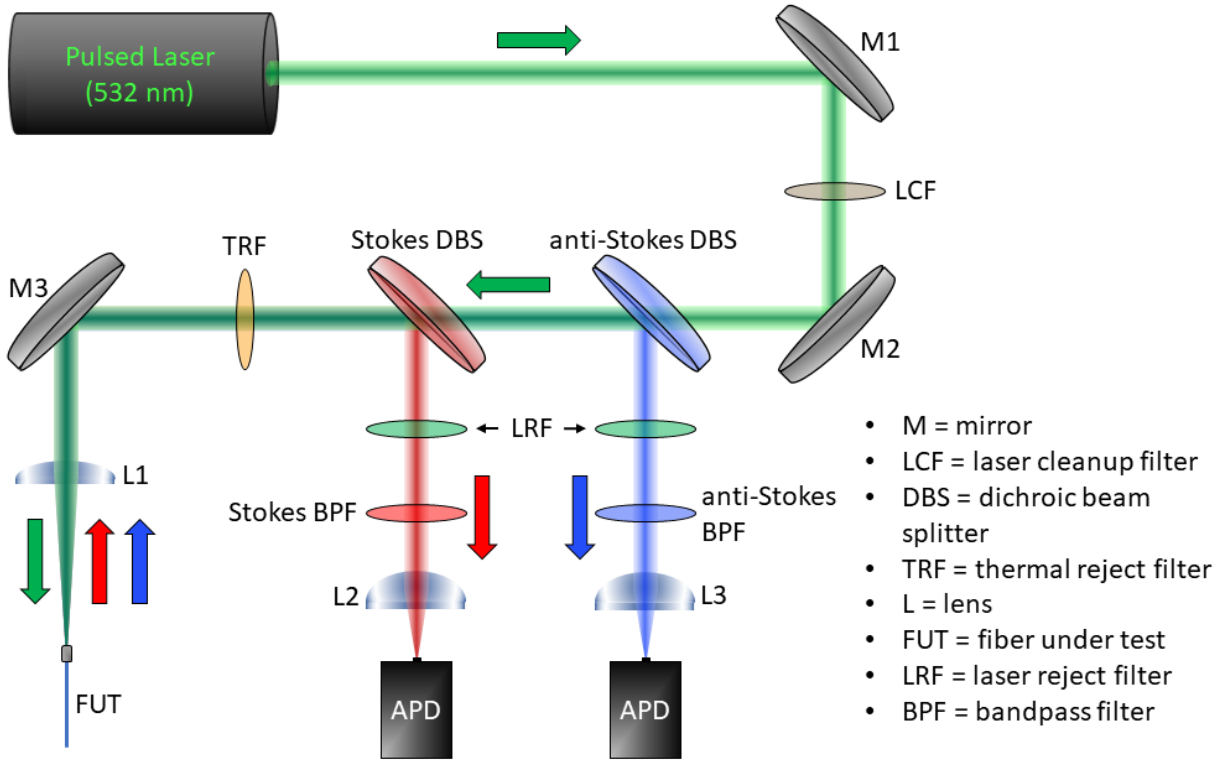

Figure 3: Optical schematic of the updated Raman DTS system. The green arrow signifies the excitation path, while the red signifies the Stokes collection path and blue the anti-Stokes collection path. The fluorescence is detected via avalanche photodiodes (APD) interfaced with an oscilloscope.

Transmissivity is quantified with respect to that of silica fiber of the same length. SC fiber is assembled with a fiber connector and connected to the fiber input labeled FUT (shown in Figure 3). Laser light is coupled into the fiber and the power is measured both before coupling into the fiber and at the output of the fiber via a power meter or spectrometer. The power of the transmitted beam is also compared to that of standard silica of the same length.

The fibers' suitability as temperature sensors are also characterized with the Raman-DTS system. The Raman-DTS system utilizes the Raman OTDR technique [21-23]. Pulsed green laser light is coupled into the fiber under test (FUT). As the laser pulse propagates down the fiber, it induces Raman scattering as both Stokes and anti-Stokes signals. The Raman signals propagate back along the fiber and are collimated with the confocal lens, L1. The Raman signals are separated from retroreflected laser light and sent along two different paths via reflection from two separate dichroic beam splitters. The intensities of the separated Stokes and anti-Stokes signals are measured with two avalanche photodiodes and an oscilloscope. Ultimately, the ratio of the magnitudes of Stokes and anti-Stokes signals is measured as a function of time and Bose-Einstein statistics are used to calculate temperature. The temperature across the length of the fiber is determined by the arrival time of the Raman pulses and its resolution is governed by the pulse width. This system's spatial resolution is on the order of 5-10 cm.

Recently, the optics of the Raman-DTS system had been upgraded to greatly increase collection efficiency of the Stokes and anti-Stokes optical paths, ultimately improving the accuracy in measured temperature [21]. Transmission spectra were obtained for every optical component and theoretical transmission matrices were calculated for each optical path. These calculations are used to estimate the collection efficiency of multiple lines within the Raman spectra the real Raman spectra emitted from the FUT from that measured by the APDs, which is modified via transmission through the optics of either path. The results of these theoretical transmission matrices are shown in Figure 4.

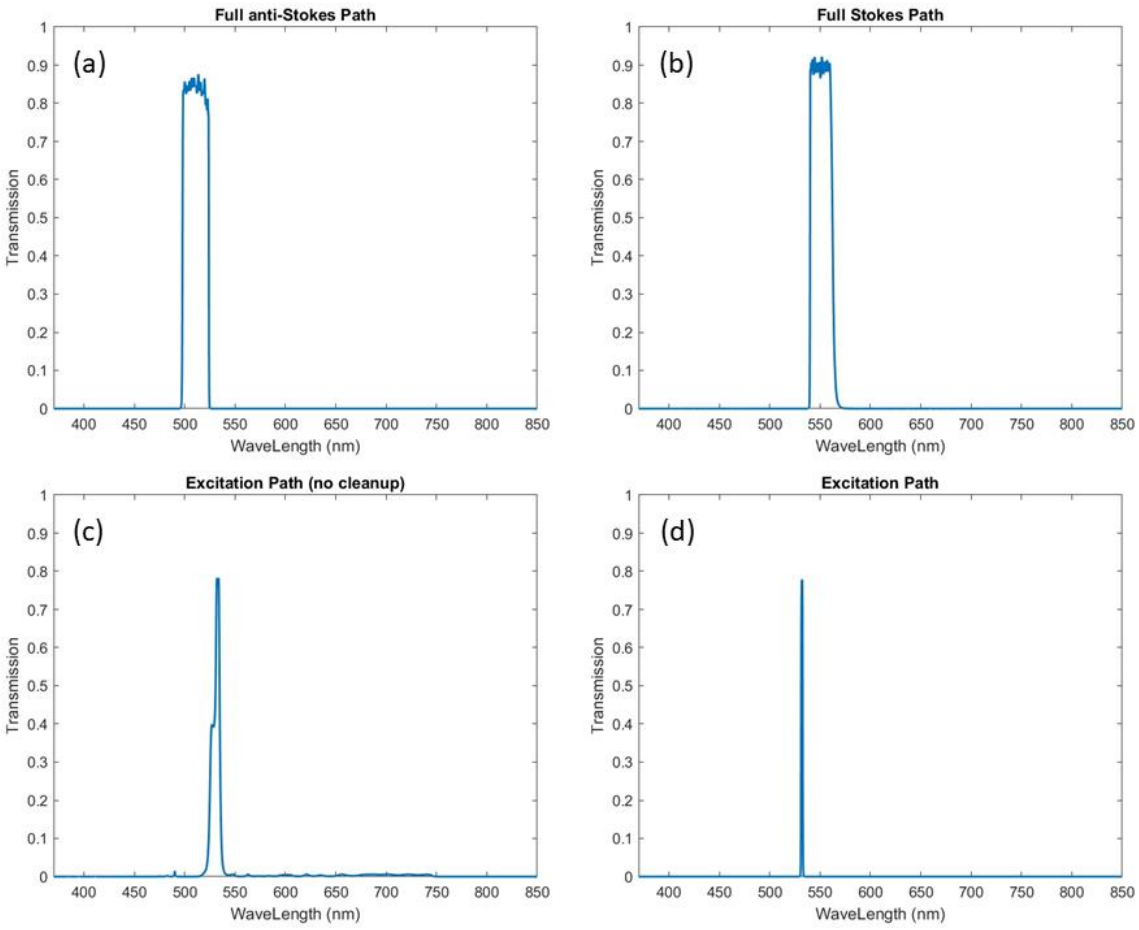

Figure 4: Theoretical transmission spectra calculated for the Raman-DTS system. (a) Anti-Stokes optical path. (b) Stokes optical path. (c) Excitation path without the laser clean-up filter and (d) with the laser clean-up filter.

Numerical Aperture (NA) Measurement System

The numerical aperture measurement system is a simple optical system built on an optical breadboard for mobility. The system involves coupling light from a HeNe laser into the FUT with a high NA lens (NA = 0.6). The output of the FUT is collimated with a lens and set incident onto a CCD camera. The NA of the fiber is then measured via the diameter of the beam incident on the CCD camera. The system was calibrated using different fibers of known NA. A schematic of the NA measurement system used to measure the NA of grown SC fibers is shown in Figure 5.

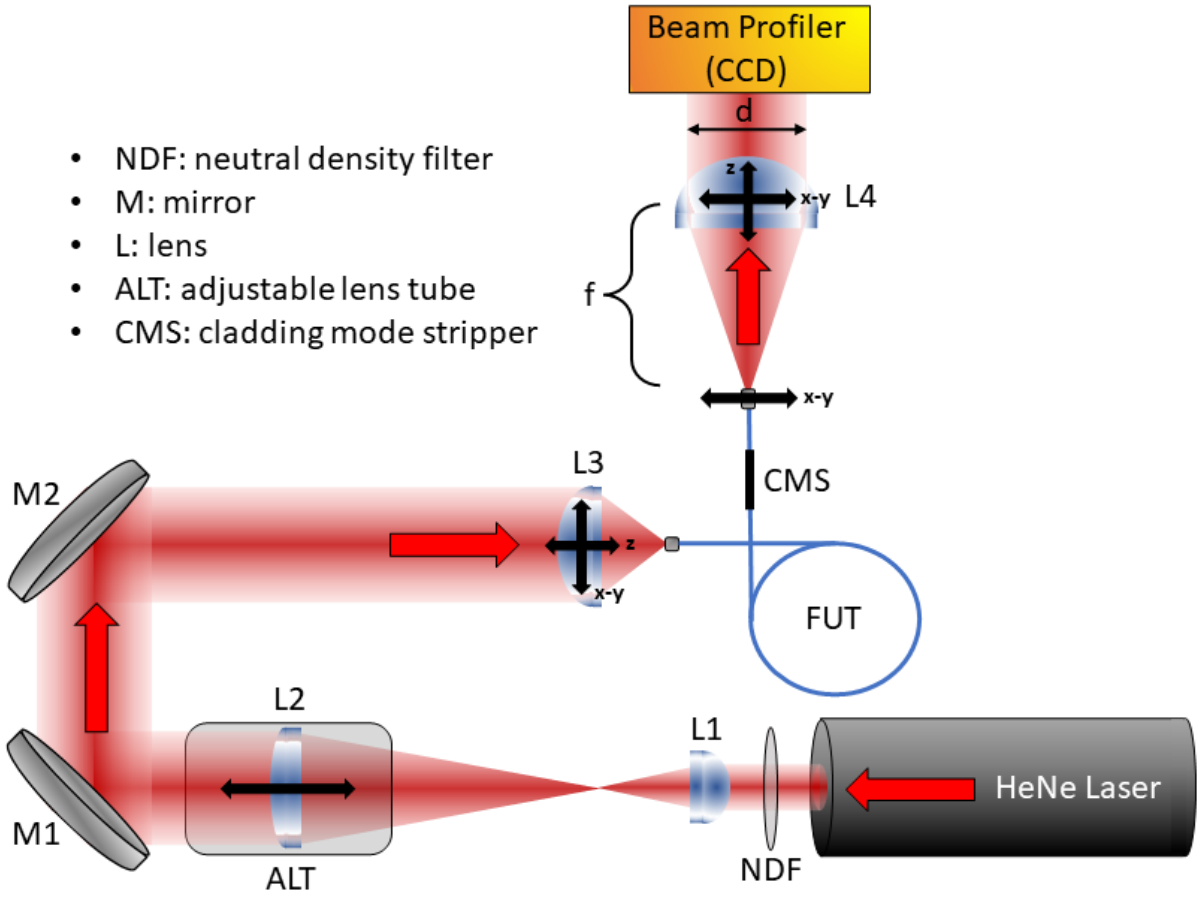

Figure 5: Schematic of mobile NA measurement system. The launch lens, L3, is maximally filled by expanding the beam with the telescope defined by L1 and L2. The collimation lens, L4, collimates the output of the FUT and sets it incident onto a CCD camera from which the beam waist, and ultimately the NA can be calculated.

3. RESULTS AND ANALYSIS

A significant amount of work has recently been conducted to improve both the hardware and LabVIEW software of both LHPG systems. Gear reducers have been installed to allow the motors to operate closer to the middle of their range, greatly increasing the precision in set angular velocities. Mechanical modifications have been made to allow for use of shorter seed fibers, increasing the percentage of fibers that are utilizable in the system. Additionally, significant improvements to the LabVIEW software allow for better measurement of the grown fiber's diameter as well as increased efficiency and reliability of the PID feedback loop that controls the motors' velocities, resulting in improved quality of grown SC fiber.

Work is ongoing optimizing the automated growth process, such that fiber can be grown for longer periods without monitoring by an operator (such as overnight growth). This has included optimization of software capabilities for maintaining the alignment of the pedestal and seed fibers, which is accomplished via monitoring the alignment with the side cameras and controlling the piezo actuators that translate the seed fiber. Additionally, work is ongoing to optimize automatic fiber reattachment capabilities for when the seed fiber either becomes detached from the molten zone or induce automatic detachment and remelting of growth that exceeds a certain threshold. That is, if a section of poor-quality fiber with a large variance in diameter is grown, the program automatically detaches the seed fiber from the molten zone, re-dips the seed into the molten zone past the defect, and restarts growth, effectively erasing the poorly grown section automatically. The goal is to scale up the system after optimization of growth parameters via implementation of the automated growth capabilities. We have established similar growth speeds to that used

previously [18-20], and with the hardware and software improvements that have been implemented, anticipate growing fiber of significantly greater quality and optical properties to that previously grown with these systems.

Since implementation of the modifications, the focus has been on improving quality of short lengths of fiber through optimization of the optics and manual fine-tuning of the control software. Roughly a dozen small pieces (1-5 cm in length) of 330 μm Ce:YAG fiber have been grown from a 1 mm diameter Ce-doped YAG feedstock rod of unknown Ce concentration. EPMA analysis is scheduled for the near future to quantify the concentration of Ce in the feedstock. During this process the recipe and experimental parameters (including motor speeds, PID parameters, laser power, etc.) have been optimized for growth of 300-330 μm YAG fiber. A microscope image of one of the grown pieces of 330 μm Ce:YAG optical fiber is shown in Figure 6.

Figure 6. Microscope image of ~330 um diameter Ce:YAG fiber. The length shown in this image is roughly 1.2 cm.

Pieces of five different grown fibers are characterized. EPMA has been conducted on all five different fibers and NA measurements were conducted on one of the fibers. Two different ~120 μm diameter fibers roughly 20 cm in length were previously grown on LHPG2: Cr-doped sapphire and Ti-doped sapphire. The transmissivities were not quantifiable with the Raman-DTS system due to such high losses in the fibers (these fibers were grown before implementation of the modifications to the LHPG systems). However, sufficient light was able to be coupled into the Cr: sapphire fiber to measure the NA with the NA measurement system, but not the Ti: sapphire fiber. The measured NA of the Cr: sapphire fiber was 0.58 +/- 0.5, which was comparable to that measured for a pure sapphire fiber of similar diameter (0.55 +/- 0.4). The other three fibers contain YAG as the host material and are roughly 300-330 μm in diameter, grown via LHPG1. One sample is a piece of Ce:YAG recently grown during the process to optimize the growth parameters for ~320-330 μm YAG growth described previously. One sample was a piece of Ho-doped ~300 μm diameter fiber that was previously used as feedstock to grow fiber in a previous work [18], and is used as a standard for comparison. The last fiber was a Nd-doped ~ 300 μm diameter fiber used as a standard for the detection of Nd,

because the first long piece of ~ 125 µm fiber grown after optimization of the experimental parameters for 125 µm growth will be grown from dip-coated Nd:YAG feedstock.

Figure 7 shows the EPMA measurements for the previously grown Ti:sapphire fiber.

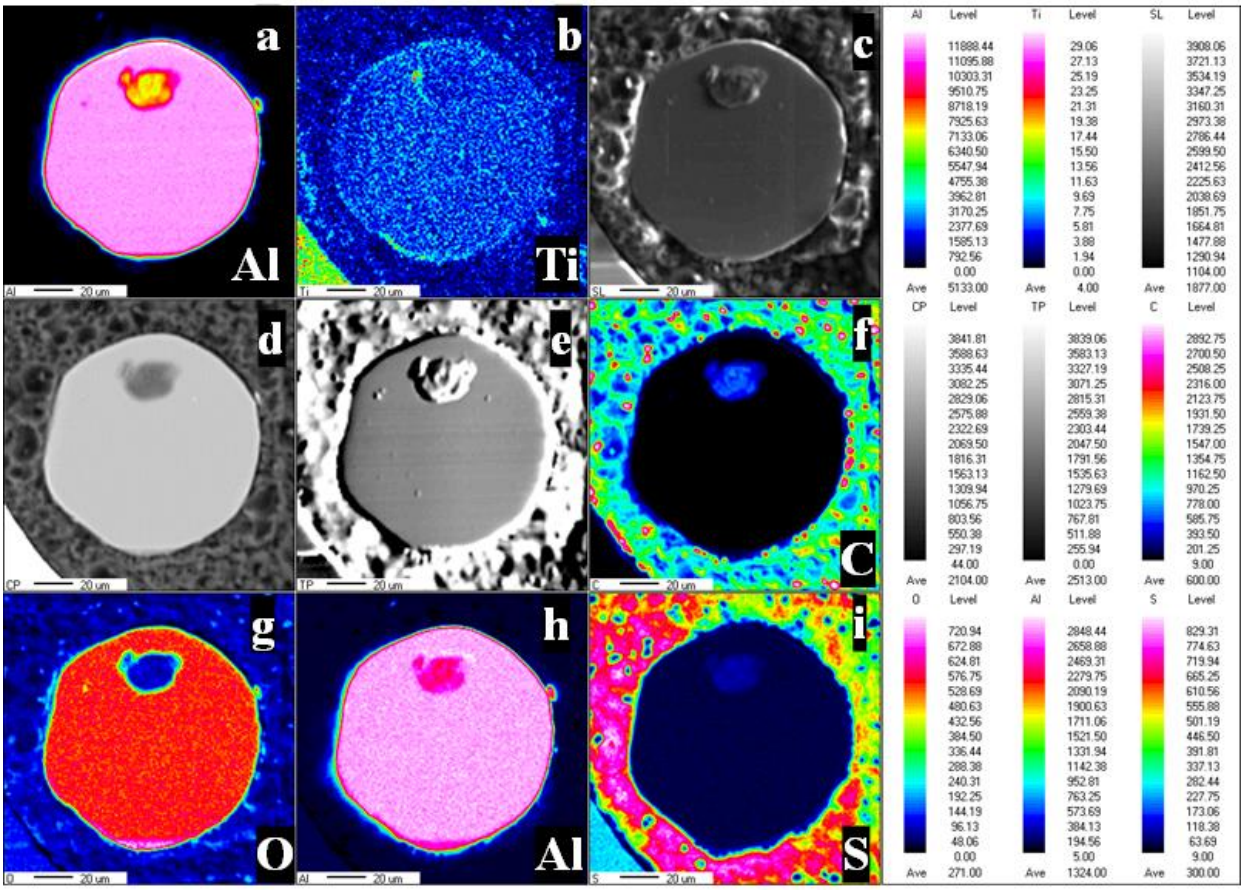

Figure 7. EPMA of previously grown Ti:sapphire fiber (a) and (b) WDS showing concentrations of Al and Ti. (c-e) Scanning electron microscopy showing SE, BSE, and TOPO, respectively. (f-i) EDS showing concentrations of C, O, Al, and S. C and S are detected in the UV-glue region surrounding the fiber.

WDS was used to detect Al and Ti, while EDS was used to detect all elemental constituents besides Ti. C and S are detected in the UV-glue region surrounding the fiber. The blotch toward the top of each image of the fiber is from a piece of dust that was not completely polished from the sample, and thus should not be interpreted as part of the fiber's composition. Ultimately, Ti was observed to be spread roughly homogenously across the fiber, with little to no segregation. Unfortunately, the EMPA results showed no presence of Cr in the Cr:sapphire fiber and it is deduced that an insufficient number iterations of the sol-gel dip-coating was applied resulting in an insignificant deposition of Cr on the pedestal fiber used for growth.

Figure 8 shows the EPMA results for the Ho:YAG pedestal fiber.

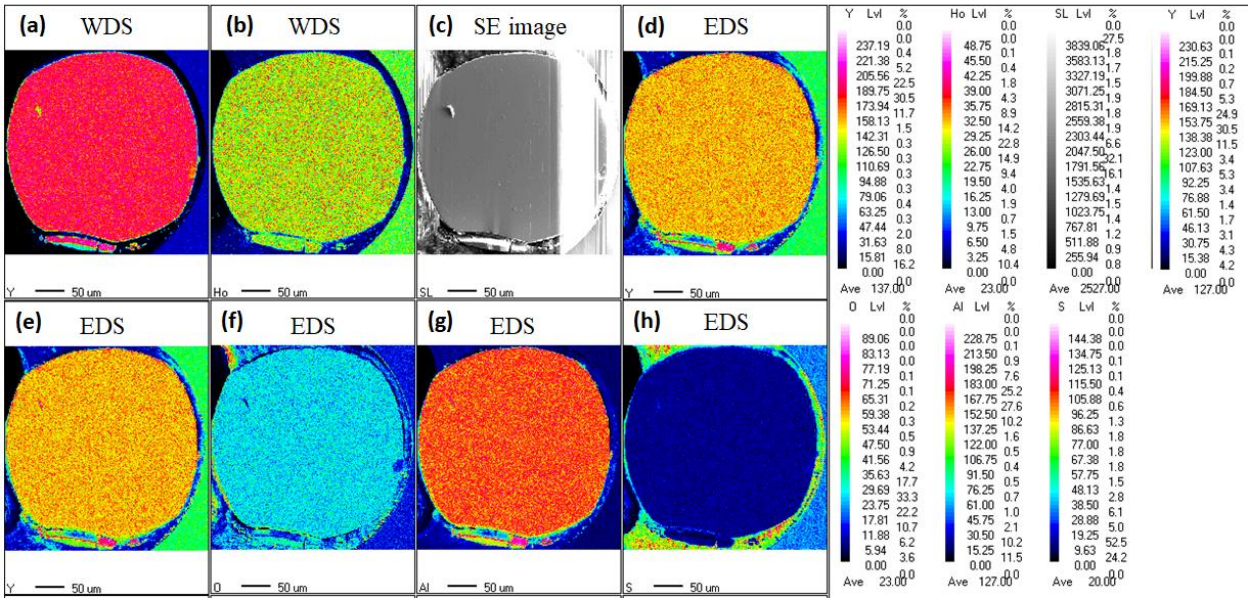

Figure 8: EEPMA of previously grown Ce:YAG fiber (a) and (b) WDS showing concentrations of Y and Ho. (c) Scanning electron microscopy SE image. (d-h) EDS showing concentrations of Y, O, Al, and S.

WDS was used to detect Y and Ho, while EDS used to detect Y, O, Al, and S. Ultimately, Ho is roughly homogenously spread across the fiber as expect.

Figure 9 shows the WDS results from the EPMA for the Nd:YAG fiber.

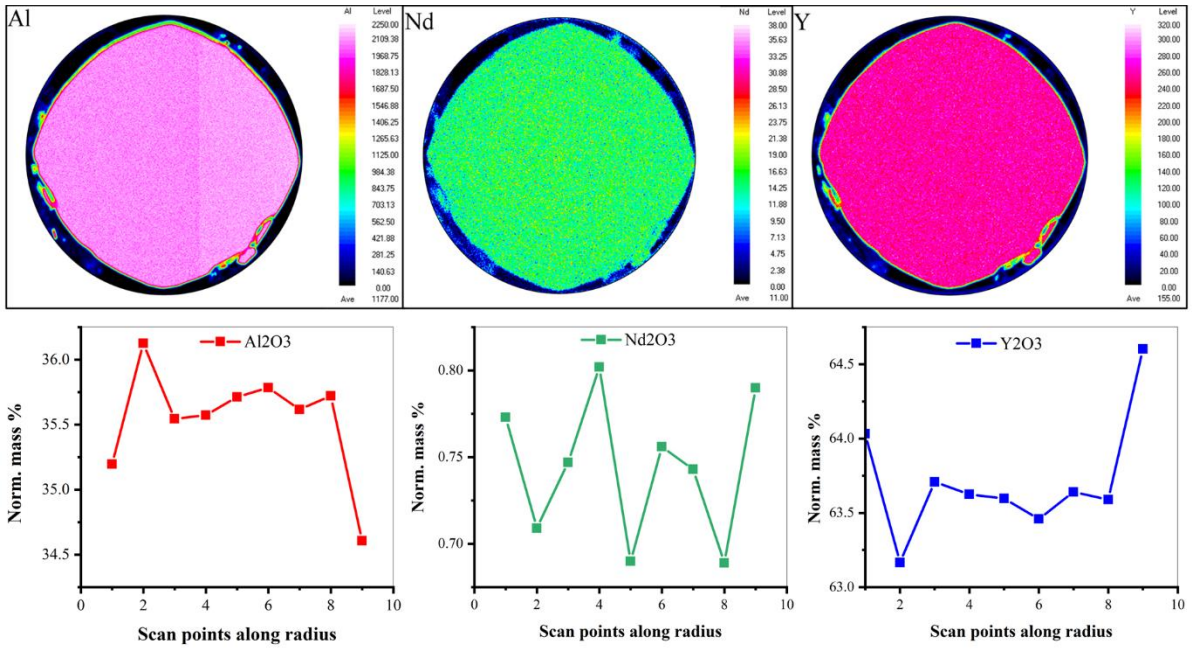

Figure 9. WDS scans showing qualitative concentrations of Al, Nd, and Y for the Nd:YAG fiber.

The WDS results for the Nd:YAG fiber show a roughly homogeneous spread of Nd across the fiber, as well as an inversely related concentration of Al and Y, as expected.

Lastly, EPMA of the recently grown Ce:YAG fiber as well as the Ce-doped YAG feedstock from which it was grown is ongoing, but preliminary results have shown the presence of Ce in the grown fiber. EPMA will be conducted across

cross-sections at different locations along the length of the fiber, paying special attention to the Ce concentration profile for locations along the fiber of differing grown diameter.

4. CONCLUSIONS

All fiber characterization techniques have been established. Calculations of theoretical transmission spectra for the optical paths in the Raman-DTS system will allow not only for more accurate distributed temperature sensing, but better characterization of grown fibers for their transmissivity and distributed temperature sensing capabilities. Preliminary EPMA analysis has been conducted and standards are set for future fiber characterization.

Recent hardware/mechanical and software modifications made to the two LHPG systems have increased the potential for improved fiber quality. One hardware modification involved implementation of gear reducers that allow the motors that control the pull and push speeds of the seed and pedestal fibers to operate closer to the middle of their range, resulting in significant improvement of the precision of the set fiber pull/push velocities. Another hardware modification resulted in decreasing the distance between the seed motors' drive shaft and the molten zone, allowing for significantly smaller seed fibers to be used in both LHPG systems. This allows not only for a larger variety of usable seed fibers, but also for a more rigid holding of the seed fiber as it is pulled up from the molten zone.

Significant modifications have been implemented to the LabVIEW software that controls both LHPG machines. These modifications have included image processing improvements that have allowed for a more reliable tracking of the edge of the molten zone as well as increased precision in the measured diameter of the grown fiber directly above the molten zone. The logic of the PID feedback loop used to maintain a constant grown diameter via control of the pedestal fiber velocity has also been modified to improve the response of the PID feedback loop to changes in diameter. Different laser lines have been explored to find those with modes closest to Gaussian as well as improvements to the optical alignment procedure discovered that guarantee an extremely symmetric and constant-volume molten zone.

Experimental parameters including values of PID constants, PID gain scheduling, image processing parameters, laser power, pull/push speeds, etc., have been optimized for ~320-330 μm YAG fiber. The experiment parameters for ~125 μm YAG fiber is almost finished. Growth rates comparable to those previously used have been established. Thus, implementation of the hardware and software modifications, improved methods for optimization of the optics, as well as improved recipes for specifically sized fibers and materials are expected to allow for a significant increase in grown fiber quality with a similar growth rate to that established previously. The first long piece of fiber grown after implementation of these improvements to the LHPG systems will be ~125 μm Nd:YAG fiber, of which at least 20 cm will be grown to be characterized via the Raman-DTS and NA measurements systems, in addition to EPMA.

DISCLAIMER

This project was funded by the United States Department of Energy, National Energy Technology Laboratory, in part, through a site support contract.

ACKNOWLEDGEMENTS

This work was performed in support of the U.S. Department of Energy's (DOE) Fossil Energy and Carbon Management's Hydrogen with Carbon Management (HCM) Research Program and executed through the National Energy Technology Laboratory (NETL) Research & Innovation Center's Sensors, Controls, and Novel Concepts Field Work Proposal.

REFERENCES

[1] H. Chen, M. Buric, P. R. Ohodnicki *et al.*, "Review and perspective: Sapphire optical fiber cladding development for harsh environment sensing," Applied Physics Reviews, **5**(1), 011102 (2018).

[2] B. Liu, and P. R. Ohodnicki, "Fabrication and application of single crystal fiber: review and prospective," Advanced Materials Technologies, **6**(9), 2100125 (2021).

[3] Y. Zhang *et al.*, "Single-crystal sapphire-based optical high-temperature sensor for harsh environments," Optical Engineering, 2004. **43**(1): p. 157-165.

[4] S. Bera, Y. Picard, M. Buric *et al.*, "Fabrication of sol-gel derived cladding for sapphire fibers and their performance evaluation under harsh environment," 11682, 84-92.

[5] S. Bera, C. D. Nie, J. A. Harrington *et al.*, "Cladding single crystal YAG fibers grown by laser heated pedestal growth," 9726, 43-51.

[6] B Liu *et al.*, "Design and implementation of distributed ultra-high temperature sensing system with a single crystal fiber," Journal of Lightwave Technology, 2018: p. 1-1.

[7] M. Dubinskii *et al.*, "Low-loss 'crystalline-core/crystalline-clad' (C4) fibers for highly power scalable high efficiency fiber lasers," Optics Express, 2018. **26**(4): p. 5092-5101.

[8] C. Burrus, J. Stone, and A. Dentai, "Room-temperature 1.3 μm cw operation of a glass-clad Nd: yag single-crystal fibre laser end pumped with a single led," Electronics Letters, 1976. **12**(22): p. 600-602.

[9] W Kim *et al.* "Cladded single crystal fibers for high power fiber lasers. in Photonic Fiber and Crystal Devices: Advances in Materials and Innovations in Device Applications X," 2016. International Society for Optics and Photonics.

[10] W. Kim *et al.*, "Hydrothermally cladded crystalline fibers for laser applications," Optical Materials Express, 2019. **9**(6): p. 2716-2728.

[11] B.A. Wilson and T.E. Blue, "Creation of an Internal Cladding in Sapphire Optical Fiber Using the $^{6} $ Li (n, $\alpha)^{3} $ H Reaction," IEEE Sensors Journal, 2017. **17**(22): p. 7433-7439.

[12] S. Bera *et al.* "Cladding single crystal YAG fibers grown by laser heated pedestal growth. in Solid State Lasers XXV: Technology and Devices," 2016. International Society for Optics and Photonics.

[13] C.M. Liu *et al.*, "Mg-Doped Sapphire Crystal Fibers Grown by Laser-Heated Pedestal Growth Method," Japanese Journal of Applied Physics, 2006. **45**(1A): p. 194-199.

[14] C.Y Lo *et al.*, "Efficient Nd:Y3Al5O12 Crystal Fiber Laser," Japanese Journal of Applied Physics, 2002. **41**(Part 2, No. 11A): p. L1228-L1231.

[15] N. Soleimani *et al.*, "Coilable single crystals fibers of doped-YAG for high power laser applications," Journal of Crystal Growth, 2014. **393**: p. 18-22.

[16] C.L. Chang *et al.*, "Simulation and experiment on laser-heated pedestal growth of chromium-doped yttrium aluminum garnet single crystal fiber," Journal of Crystal Growth, 2011. **318**(1): p. 674-678.

[17] R. Simura, A. Yoshikawa, and S. Uda, "The radial distribution of dopant (Cr, Nd, Yb, or Ce) in yttrium aluminum garnet (Y3Al5O12) single crystals grown by the micro-pulling-down method," Journal of Crystal Growth, 2009. **311**(23-24): p. 4763-4769.

[18] S. Bera, P. R. Ohodnicki, M. Buric, *et al.*, "Dopant segregation in YAG single crystal fibers grown by the laser heated pedestal growth technique," Journal of Crystal Growth, 2020. **547**, 125801.

[19] S. Bera *et al.,* "Optimizing alignment and growth of low-loss YAG single crystal fibers using laser heated pedestal growth technique," Applied Optics, 2017. **56**(35): p. 9649-9655.

[20] S. Bera *et al.*, "Growth and lasing of single crystal YAG fibers with different Ho3+ concentrations," Optical Materials, 2018. **75**: p. 44-48.

[21] G. Lim *et al.*, "Improvement of signal-to-noise ratio for Raman distributed temperature sensing on gas turbines." Optical Waveguide and Laser Sensors II. Vol. 12532. SPIE, 2023.

[22] Y. Liu, L. Ma, C. Yang *et al.*, “Long-range Raman distributed temperature sensor with high spatial and temperature resolution using graded-index few-mode fiber,” Opt. Express 26(16), 20562–20571 (2018).
[23] B. Liu, Bo *et al.*, "Design and implementation of distributed ultra-high temperature sensing system with a single crystal fiber." Journal of Lightwave Technology 36, no. 23 (2018): 5511-5520.